

Vibrational Mechanism for Primary Charge Separation in the Reaction Center of *Rhodobacter Sphaeroides*

Nikolaj Ivashin*

Institute of Molecular and Atomic Physics, National Academy of Sciences, 70 F. Skaryna Avenue,
220072 Minsk, Belarus

Sven Larsson

Department of Physical Chemistry, Chalmers University of Technology, S-41296 Göteborg, Sweden

Received: September 7, 2001; In Final Form: December 4, 2001

Geometry, reorganization energy, and vibrational and electronic spectra of pigment molecules in bacterial photosynthetic reaction centers (*Rhodobacter sphaeroides*) are determined using quantum chemical methods. B3LYP calculations on a slightly truncated form of bacteriochlorophyll *a* give vibrational modes at 23, 40, 64, and 128 cm⁻¹, which we conclude correspond to those seen in resonance Raman (RR) spectra of reaction centers with labeled cofactor atoms, and, as oscillations, in optical transient spectra. On heavy atom substitution at the axial imidazole connection to the protein, a mode with considerable contribution of bending deformations of the whole imidazole is transformed to predominantly rocking modes of the whole macrocycle at 10 cm⁻¹. Other modes, with significant character of out-of-plane, torsion, and in-plane motion of the acetyl side group of ring I, are less changed. We show that there is a connection between the mentioned modes, particularly the torsion mode of the acetyl group of ring I, and electron transfer and intensity in RR spectra. Coupling energies, calculated at a transition state between P*B_A and P⁺B_A⁻, are found to agree reasonably well with experimental data. The lower activity of the B-side compared to the A-side is caused partly by less electronic overlap between P_A and B_B than between P_B and B_A and partly by higher energy of the P⁺B_B⁻ state than of the P⁺B_A⁻ state. Finally, we compare to results for other species and for mutants. Measured rates correlate well with the energies of the P*B_A (and P*B_A^{*}) states relative to the energy of the intermediary P⁺B_A⁻ state.

1. Introduction

The primary processes of photosynthesis have been studied by photophysical methods for more than two decades.¹ Shuvalov et al. proposed in 1978 on the basis of time-resolved transient absorption experiments on the reaction center of *Rhodospirillum rubrum*, that the excited electron is transferred from a “special” pair, P, of bacteriochlorophyll (BChl) via an “accessory” BChl to a bacteriopheophytin (BPh) moiety.² This picture, suggesting an intermediate step in which the electron is located at an accessory BChl, also holds for the now better-studied reaction center (RC) of *Rhodobacter (Rb.) sphaeroides* and is generally accepted as correct.^{3–6} After structures of bacterial RCs had been determined by crystallographic methods⁷ (Figure 1), it was shown that only the L part of two almost equivalent L and M protein units of the RC is directly involved in charge separation.⁸ The special pair P is formed from two BChl *a* molecules, P_A and P_B. Henceforth, we will denote by P_A the BChl *a* molecule attached to the L part of the protein by hydrogen bonds and an axial imidazole ligand belonging to His L173. The molecule identified as the accessory BChl *a* molecule is attached to the L part in a similar way and denoted B_A, while BPh *a* with no axial imidazole, but in direct contact with B_A, is denoted Φ_A. The corresponding chromophores on the M side are called P_B (attached to His M202), B_B, and Φ_B, respectively.

The charge-separation process and subsequent electron-transfer (ET) steps have been studied using various theoretical models, particularly the Marcus model⁹ and vibrational overlap models.¹⁰ More or less accurate quantum chemical methods have been used to calculate wave functions, energies, and relevant

coupling parameters.^{11–15} The small magnitude of the direct electronic coupling between P and Φ_A compared to the rather large couplings between P and B_A and between B_A and Φ_A supports the Shuvalov two-step model.^{2,12} In fact, the two-step model is the only of the two models that can explain the high efficiency of the charge-separation process in avoiding local triplet formation at P. In the one-step model, back electron transfer to P from a spin-flipped P_A⁺B_AΦ_A⁻ state would be possible with about the same rate as forward transfer. The activation barrier for the back reaction should be no larger than the one for the forward reaction because energetically the lowest P* triplet state is approximately as much below the charge-separated state as the charge-separated state is below the lowest P* singlet state. The electronic coupling is the same because the same molecular orbitals (MO) are involved as in the forward transfer. But, because this pathway has a much too small electronic factor to allow fast ET,¹² back reaction to the triplet state is very slow in reality. The contribution to the electronic factor via B_A can be estimated if the latter pigment molecule is left out of the calculation and is in fact insignificant.¹² The direct coupling via the protein is also too small. The conclusion is that the B_A⁻ state has to be involved as a real intermediary, so that there is an increase of electron density on the accessory BChl during some time period after excitation of P.

In previous papers,^{12,13} we calculated electronic couplings between several chromophores of the RC. The results agree with other papers,^{14,15} in which ab initio methods are used in critical parts. In the present paper, we want to study the coupling between ET and vibrational dynamics. Oscillatory components

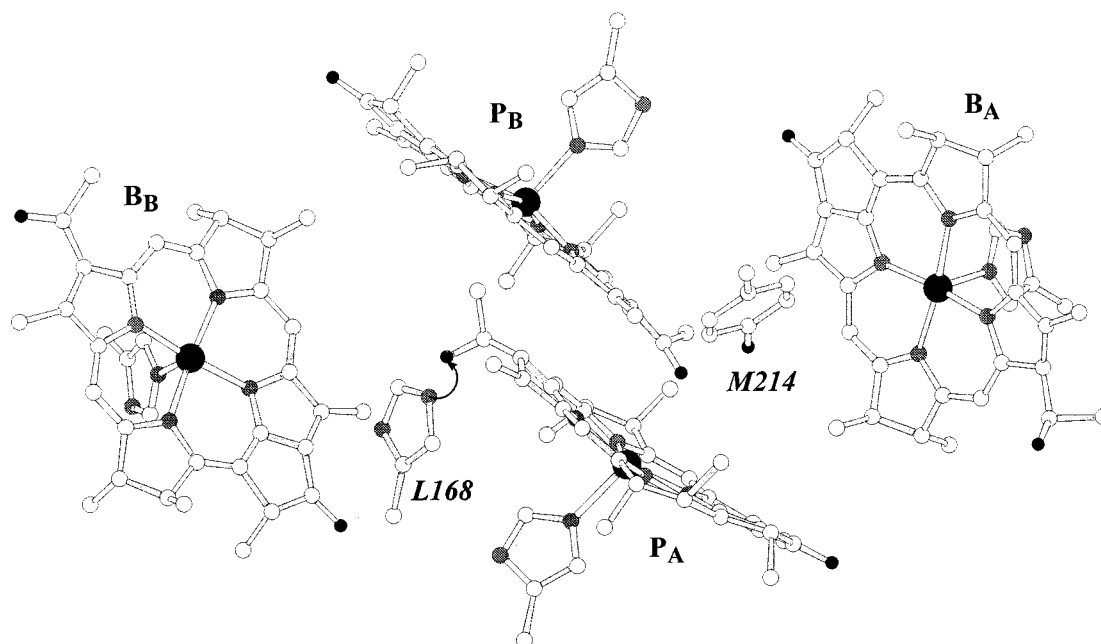


Figure 1. Pigments of primary charge separation. P = P_AP_B is the special pair of bacteriochlorophyll *a* (BChl *a*); B_A and B_B are accessory BChl *a*'s. The histidine L168 imidazole side group forms hydrogen bonds with P_A (arrow). The corresponding group on the B-side, M214, does not form a hydrogen bond.

have been found in time-resolved spectra of reaction centers,^{16–24} which are interpreted as due to coherent vibrational wave packet motion. Vos et al. first found subpicosecond oscillations in the stimulated emission kinetics of P^{16–18} of unknown origin. Later, Streltsov et al. found similar oscillations in the absorption spectrum of B_A, which were connected to electron transfer (ET).^{20,21} The origin of these oscillations was ascribed to nuclear motions in the protein or relative motion between the monomers of P. Spörlein et al. found vibrational coherence in the P⁺B_A[−] region at 1020 cm^{−1} but related the latter to stimulated emission or absorption to higher excited states.²² Yakovlev et al., who found similar oscillations, related them to ET,²³ however. More recently, Vos et al. found oscillations in the transient kinetics at 788 nm, corresponding to electrochromic influence on the bacteriochlorophyll monomer absorption as a result of formation of the P⁺Φ_A[−] state.²⁴ These oscillations are strongly modified in mutants, for example, the YM210W mutant.^{21,24} However, it is still unclear what the reason for the oscillations is or whether they are connected to ET. It has been suggested though that the acetyl group of ring I may be involved because it is conjugated with the π -system of the macrocycle,²⁵ making it credible that its motion is coupled to the dynamics of the π -electrons.

Resonance Raman spectra (RR) of bacterial reaction centers show a number of low-frequency lines.^{26–31} The Raman scattering cross sections at excitation in the monomer B and H absorption regions are 6–7 times larger compared to those of analogous modes at excitation in the P absorption region at 278 K. The Raman intensities corresponding to monomers are increased by a factor 3–4 at 95 K, while for the dimer, the intensity is almost unchanged.²⁷ Cherepy et al. proposed as an explanation that the excited state of P is damped by very rapid (<30 fs) electronic relaxation processes, possibly due to mixed electronic components in the P* state (charge transfer + excitation). Similar proposals have been made to explain hole-burning experiments³² or theoretically.^{33,34} In the low-frequency region, however, where the RR intensity is small for the monomers, the dimer spectrum contains several rather strong lines at 36, 70, 96, 127, and 145 cm^{−1}. RR data combined with a semiem-

pirical calculation of the BChl *a* vibrational spectrum show that strong coupling of modes is consistent with a structure of the dimer in which overlap occurs primarily in the region of ring I.³⁰ The lowest mode found in RR spectra of P at 36 cm^{−1} was assigned to out-of-plane deformation of the C2-acetyl group of ring I. This RR frequency was suggested to be involved in ET.³⁰

Another important finding concerning the dynamics of the charge separation is that the rate constant increases as the temperature is lowered.³⁵ In calculations of the charge-separation rate, it is important to know which vibrational modes are important for promotion of ET.

Recently, it has become possible to apply *ab initio* calculations on quite large biochemical systems to optimize the structure for a part of the protein.^{14,15,34,36–41} A vibrational spectrum has been calculated using a density functional method and compared in great detail to RR spectra⁴⁰ but did not provide any results in the low-frequency region. The work of Hutter et al.³⁸ contains a thorough discussion about the optimization problem for the protein using semiempirical methods. The electrostatic influence from the protein has been treated using the finite difference Poisson–Boltzmann equation.⁴²

In the present paper, we will first examine which structural changes are connected to ET using *ab initio* calculations on slightly truncated, neutral and ionic BChl *a* molecules. The vibrational spectrum is calculated for truncated forms of BChl *a*, including some groups of the protein in the discussion. We find that the low-frequency modes, mainly belonging to torsional, in-plane and out-of-plane motion of the side groups, are indeed coupled to ET. Finally, we calculate the rate using a wave packet model⁴³ and make conclusions regarding the mechanisms for charge separation.

2. Optimization of Structure

We used three different levels of optimization. In exploratory calculations, we added hydrogen atoms to the crystallographic structure using molecular mechanics⁴⁴ and semiempirical programs^{45,46} in HyperChem⁴⁷ (MM+,⁴⁴ PM3,⁴⁵ AM1⁴⁶). The positions of the hydrogen atoms were optimized using molecular

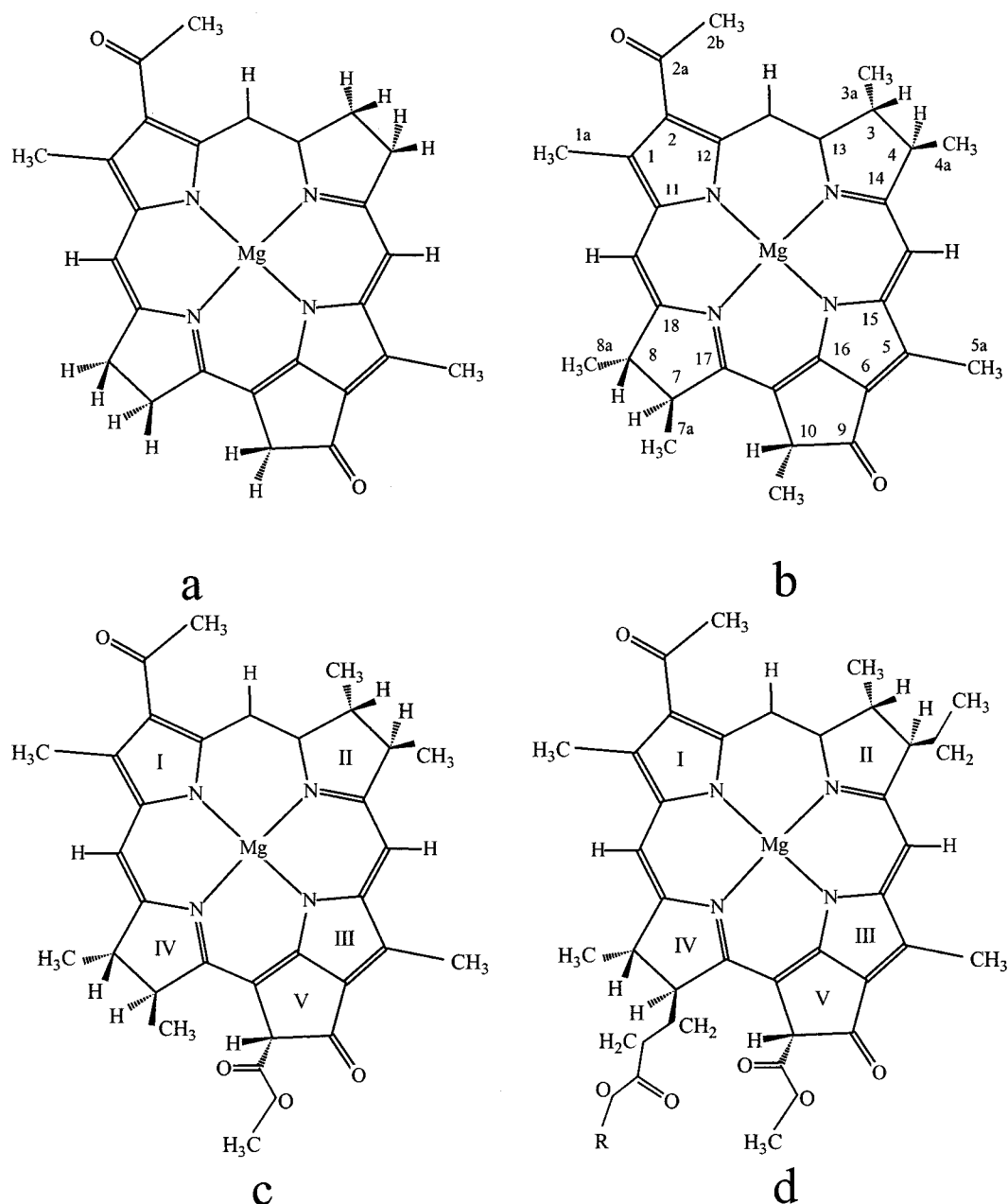


Figure 2. Truncated forms of BChl *a* studied on the B3LYP/6-31G* level: (a) with 55 atoms, (b) with 70 atoms, and (c) with 82 atoms included. The true structure is given in panel d. The imidazole group ($C_4N_2H_3$) connected to Mg is not shown in the 82-atom model and natural system.

mechanics (MM+) while retaining the crystallographic structure for the heavier atoms.

At a higher level of exploratory calculations, we optimized structures using the semiempirical PM3 method.⁴⁵ This model, as well as the AM1 model,⁴⁶ has the potentiality to determine the structure of the protein backbone, including CC and CN bond lengths. If the models are applied to the special pair (in free space), the result does not agree with the crystallographic structure, however. Hutter et al.,³⁸ using the AM1 model, were forced to use constraints to conserve the dimer structure according to crystallographic data. Apparently, full understanding of the interaction between the prosthetic groups and the protein is still not at hand. We therefore decided to use the crystallographic structure for the heavier atoms and optimize the hydrogen geometry as described above in the cases when only rough structural data is needed.

Unfortunately, the semiempirical PM3 and AM1 methods are too crude to determine the lower part of the vibrational spectrum.

The potential energy surface (PES) for torsional motion of the side groups is simply not good enough. However, it is possible to get an idea about the mixing of different low-frequency modes as well as modifications due to the restriction of the motion at the axial ligand, the phytyl chain, or the hydrogen bonds.⁴⁸

At the highest level of accuracy, we used the B3LYP density functional method⁴⁹ within Gaussian 98⁵⁰ with the 6-31G* basis set to optimize the structure of three truncated forms of BChl *a*. In the first calculation (Figure 2a), 55 atoms were included. The acetyl and methyl groups of ring I were kept. The substituents of the outer carbons of rings II and IV, which are not a part of the conjugated system, were replaced by hydrogen. The methyl group of ring III was kept. The methyl carboxyl group of ring V, which is not part of the conjugated system, was replaced by hydrogen. The carbonyl group of this ring was kept. The geometry of the positive and negative ions was optimized. The results are given in Figure 3.

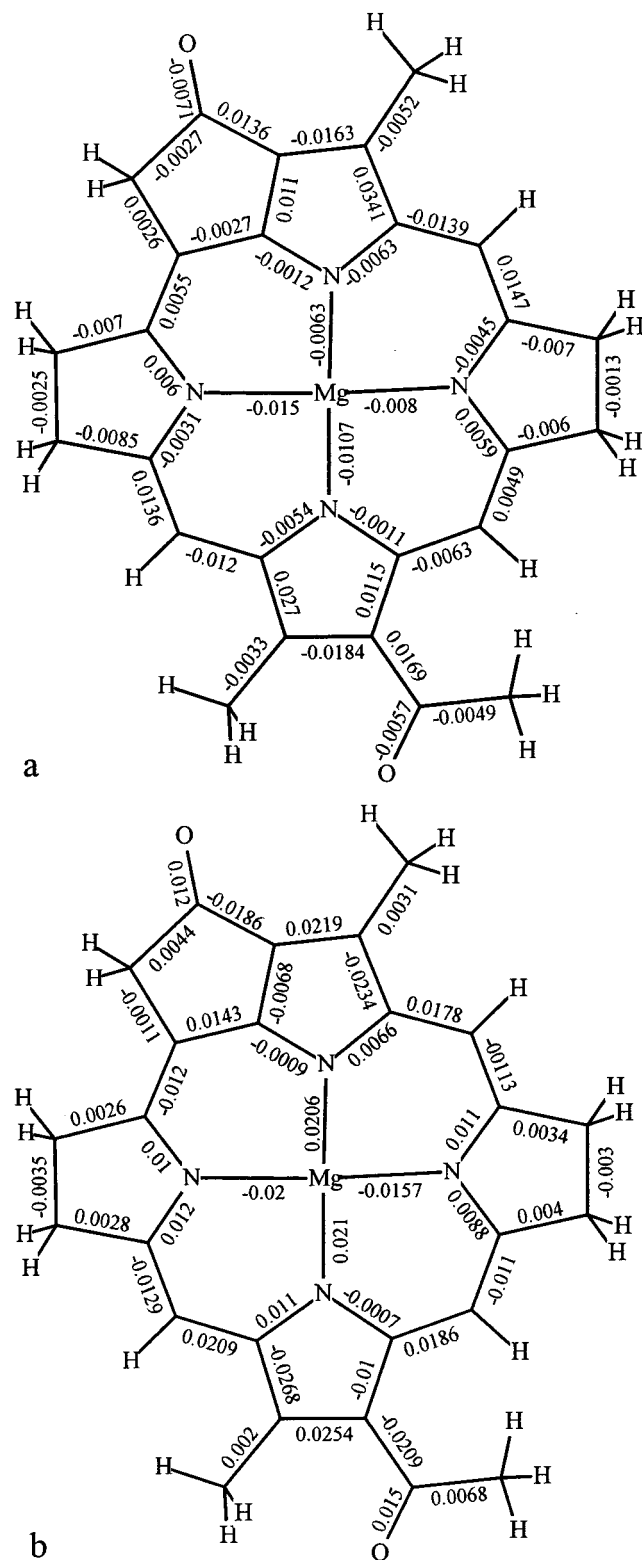


Figure 3. Geometric changes in bond lengths of the 55-atom model when BChl *a* is oxidized (top) or reduced (bottom) (B3LYP calculation using the 6-31G* basis set).

To study the consistency of the calculated vibrational energies, we carried out another B3LYP calculation with the 6-31G* basis set on a larger system containing 70 atoms. In this calculation, the two natural methyl groups of rings II and IV were included and three additional methyl groups instead of hydrogen to represent the natural substituents on rings II, IV, and V. (Figure 2b). Because replacement of hydrogens by methyl groups cannot

be expected to change CC and CN bond lengths, no new calculations for the ions were made for the 70-atom system. Finally, in a third B3LYP calculation using the 6-31G* basis set, we also included the axial imidazole group in the second structure and also the natural methoxy carbonyl side group at position 10 of ring V, in total 82 atoms. The latter group was included because it turned out to interact with the imidazole group in model calculations.

Later, we found it important to improve the description of the low-frequency modes by including 24 of the 68 atoms of the phytol chain and the ethyl group of ring II. Because of the size of this system, the basis set had to be reduced to 3-21G.

CC and CN bond lengths are structural elements that are recognized as coupled to ET. The bond-length increase or decrease at oxidation or reduction is proportional to the negative of bond-order change and can be obtained by any method capable of providing good HOMO and LUMO. The B3LYP calculation should be very reliable in this respect. We find that the CC, CN, and CO bond-length changes are always smaller than 0.03 Å (Figure 3). This means that the contribution to the reorganization energy is small. The latter is obtained as

$$\lambda = \sum_{\text{bonds}} \frac{1}{2} k_i \delta R_i^2 \quad (1)$$

Assuming a realistic average value of the CC, CN, CO, and stretch frequencies (and using a calculated value for the MgN force constant), we obtained $\lambda = 0.17$ eV for adding one electron to the neutral molecule and $\lambda = 0.13$ eV for removing one electron. Direct calculation of λ , where the energies of the ions are calculated at the equilibrium positions of the neutral ground state and the energies of the neutral ground state were calculated at the equilibrium geometry of the ion, was carried out for the truncated geometry (Figure 2a). We found 0.124 eV for adding one electron to the neutral molecule and 0.125 eV for removing one electron from the negative ion and 0.084 eV for adding one electron to the positive ion and 0.083 eV for removing one electron from the neutral molecule. The differences from the values obtained using eq 1 (0.17 and 0.13 eV, respectively) are about 0.05 eV, which is a quite small error in a calculation of reorganization energy.

The reorganization energy for excitation to the locally excited S_1 state may also be estimated. This state has a major component of HOMO \rightarrow LUMO excitation and both of these MOs are π orbitals. Because, furthermore, bond-length change is proportional to bond-order change, we conclude that the bond-length changes at excitation may be estimated by summing the bond-length changes for removing one electron and the bond-length changes for adding one electron. The changes in a particular bond length for removing and adding one electron cancel out to a large extent, and the final reorganization energy, using eq 1, is only 0.035 eV.

The results for the excited state of the monomer cannot be easily transferred to the special pair dimer. The excited state of the latter has a considerable contribution of charge-transfer character.³³ The lowest singlet state is mainly a transition from a HOMO, mainly located on P_A to a LUMO located mainly on P_B . The fundamental reason for this is that the acetyl group of P_A is distorted out of the plane of conjugation due to hydrogen bonding.

Figures 4–6 show geometry changes in one of the side groups when electrons are added or subtracted. As is seen, the changes correspond closely to a rather large torsion motion of the acetyl group (Figures 4 and 6). Figure 5 shows an appreciable change

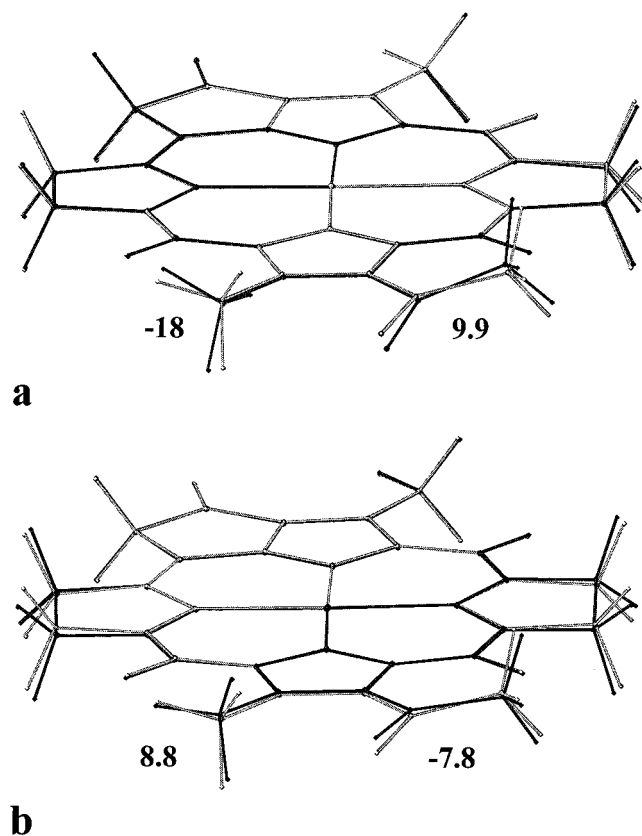


Figure 4. Geometry changes in torsion angles of the 55-atom model when BChl *a* is (a) oxidized or (b) reduced (B3LYP calculation using 6-31G* basis set).

of the angle between the axial imidazole ligand and the plane of the macrocycle ($\sim 4^\circ$) on reduction, which corresponds to a rocking motion of the macrocycle; it is assumed that the imidazole ligand is fixed to the protein. These changes are connected to small force constants, and consequently, the associated reorganization energy is small.

Even if the calculation of an accurate PES for rotations of side groups is often connected to large relative errors, we believe that the changes in dihedral angles in this case are quite reliable. Because the LUMO is bonding in the region of the acetyl group, there is a decrease of the dihedral angle for acetyl for the negative ion when the LUMO is being occupied. The change of the equilibrium geometry from the $P^+B_A^-$ state to the P^+B_A state defines the activating motion for ET from P to B. In a sense, this motion is due to a “coupling” between electronic and nuclear motion for the primary charge separation process.

There is a quite significant change of the angle between the axial imidazole group and the plane of the macrocycle on reduction. This results in activation of the rocking motion of the macrocycle at ET.

3. Calculation of Vibration Spectrum

Because ET takes place on the first excited PES, the vibrational calculation should, in principle, be performed at the equilibrium position on that energy surface. The experimental data that we will compare to also refer to that surface. Unfortunately, it is impossible at the present to carry out vibrational calculations on excited PESs. Furthermore, it is not yet established what the first excited PES corresponds to for each single chromophore. Because we found above that the reorganization energy is small from ground state to excited state,

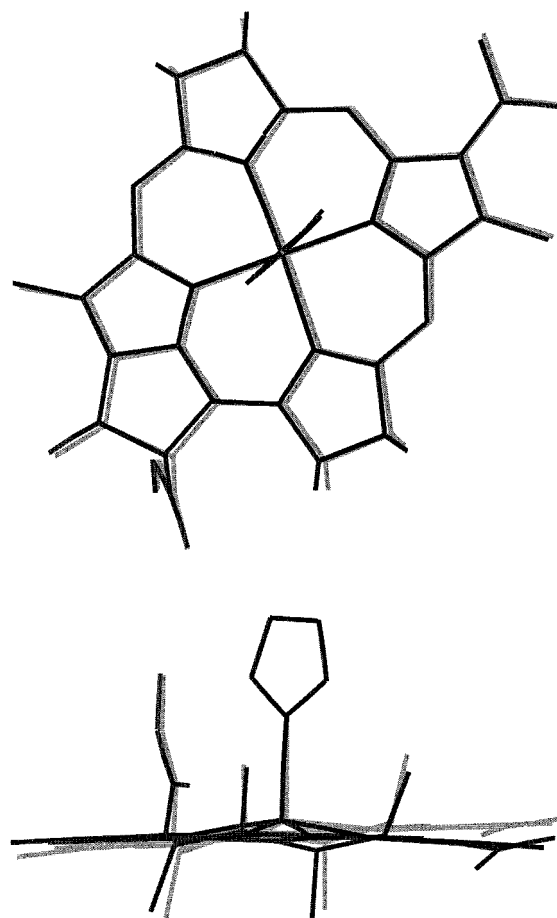


Figure 5. Reduction of BChl *a* (82-atom model) causes small but relevant geometry changes: neutral molecule, dark; negative ion, gray. Imidazole ring is fixed in space.

we believe that a vibrational calculation for the ground state is relevant also for the excited state.

Exploratory calculations of the vibration spectrum of a truncated BChl *a* monomer were carried out using the semiempirical methods of the HyperChem programs⁴⁷ to get a general idea of how much of the system needed to be included to get acceptable convergence. The calculated lower frequencies involve out-of-plane, in-plane, and torsional motion of the side groups as well as ruffling, saddling, and doming of the macrocycle. If the imidazole axial ligand is included, the rotation and bending of the latter group relative to the macrocycle belongs to the low frequencies. Another important motion is the relative rotation of the phytyl chain and the macrocycle. We also found that the frequencies of the ring I side groups are comparatively unaffected by the truncations described in the previous section. Unfortunately, the semiempirical methods do not give a sufficiently accurate PES to predict vibrational energies accurately, particularly not torsional motions.

B3LYP calculations using the 6-31G* basis set lead to the frequencies shown in Table 1. We believe that the method is quite accurate to estimate the frequencies for the possibly unrealistic truncated systems in free space. The major errors are thus in the truncations. In the 55-atom calculation, modes of low frequency were found at 24, 35, 60, and 137 cm^{-1} . The 24 cm^{-1} mode has a large contribution of acetyl out-of-plane motion. Torsion and in-plane motions of the acetyl group appear mainly to the 35 and 137 cm^{-1} modes, respectively. The description of the modes is simplified because all side groups are involved to some extent and couple to the acetyl modes. In

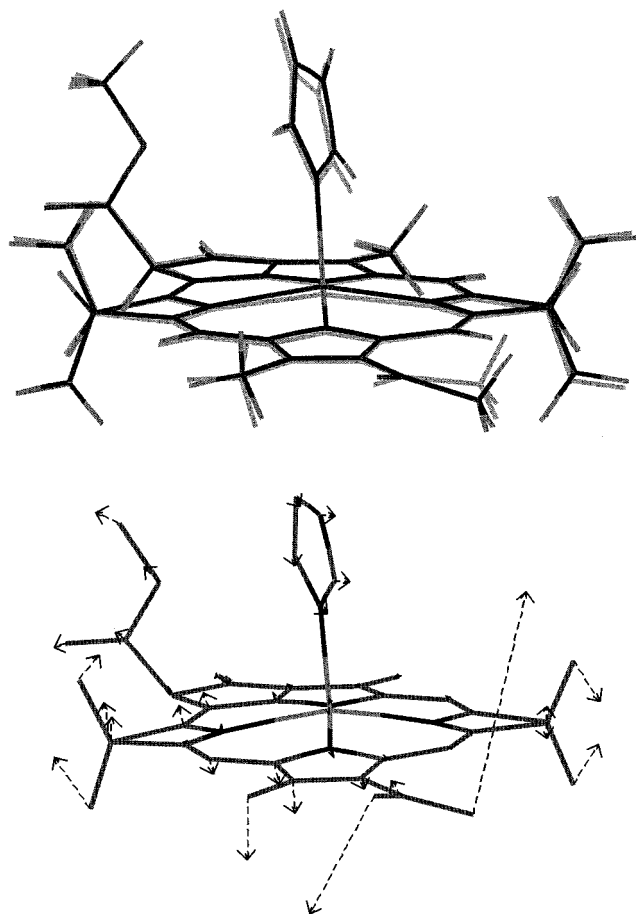


Figure 6. Results for 82-atom model: (top) geometry changes between neutral molecule (dark) and negative ion (grey) obtained by fixing macrocycle; (bottom) calculated torsion mode, mainly of ring I acetyl group, at 37 cm^{-1} .

particular, the methyl group on the same ring I couples strongly to the motions of the acetyl group.

The equilibrium geometries for the three truncations are slightly different. For example, the dihedral interplane angle measuring the torsion of the acetyl group of ring I is 14.6° in the 55-atom calculation, 12.6° in the 70-atom calculation and 18.7° in the 82-atom calculation. In all truncations, there is a mode at 24 cm^{-1} , but the character of the mode varies. In the 55- and 82-atom calculations, the latter mode consists of out-of-plane motion of the whole acetyl group. In the 70-atom calculation, however, the 24 cm^{-1} mode has a major contribution from motion of only the methyl part of the acetyl group. The out-of-plane motion of the carbonyl group is in this case mainly in modes with slightly different frequencies.

The main part of torsional motion of the acetyl group is at 34 and 38 cm^{-1} in the 55- and 82-atom (Figure 6) calculations, respectively. In the 70-atom calculation, however, only 27 cm^{-1} is obtained for the mode closest to acetyl torsion, which illustrates the difficulty in obtaining converged results for this large system.

The calculation including the axial imidazole predicts some modes that do not appear to be realistic for the natural system. To simulate the natural situation where the imidazole group is attached to a more or less fixed protein, we introduced an atomic mass of 200 on the hydrogen atom bonding to the imidazole carbon atom farthest away from the Mg atom. The kinematic damping of the axial imidazole induces rocking motion of the whole BChl molecule at low frequencies. One of them, at 6

cm^{-1} , is out-of-plane motion around an axis of the macrocycle perpendicular to the imidazole axis, connecting ring I and ring V. The motion around the perpendicular axis of the macrocycle plane is found at 13 cm^{-1} (Figure 7).

It should be noted that the calculated mode at 13 cm^{-1} contains a considerable contribution from ring I out-of-plane motion, thereby varying the distance between two halves of the dimer. This was earlier proposed by several groups to be of a great importance for electron transfer, but the proposed frequency (100 cm^{-1}) appears to be too high.

It is reasonable to suggest that the macrocycle swinging can be induced not only by the imidazole connection to the residue, but also by the phytyl chain. To check this possibility, the vibrations for the model with part of the phytyl chain (containing 24 atoms, the natural number is 68) were calculated on the B3LYP/3-21G level. The effect is pronounced and increases considerably after increasing the mass of the end of the tail to 100 atomic mass units. Modeling at the PM3 level shows that the natural tail has suitable mechanical properties for inducing motions of the whole macrocycle relative to the tail (see also ref 48). One of the induced motions has considerable contribution of the macrocycle torsion motion around the neighboring part of the tail. This motion involves ring I out-of-plane displacements, which means that the distance between the monomers can vary in the same way as in the cinematic damping of the axial imidazole motion.

The data given above shows an important role of the phytyl chain and axial imidazole binding to protein in forming the lowest frequencies of the macrocycle. We are trying now to improve the calculations further to get more information concerning the frequencies of the rocking motions and their influence on other modes.

As has been shown in the previous section, change of the torsion angle of the acetyl group of ring I accompanies oxidation or reduction of the macrocycle. This means that the acetyl group torsion mode may be involved in the charge separation. This will be further discussed in section 5.

On the basis of the 82-atom model, it is reasonable to assign the oscillation at about 12 cm^{-1} , obtained experimentally by Streltsov and co-workers,^{20,21} to rocking motion of BChl *a* macrocycle. Another possible candidate, at 21 cm^{-1} , has a considerable contribution of out-of-plane motion of the acetyl group of ring I. The choice of rocking motion is to be preferred on the basis of the geometry changes that accompany the molecule at reduction (Figure 5), which should imply a prominent oscillatory component in the spectrum.

The rocking motion of the whole macrocycle, tilting motion of ring I, and acetyl out-of-plane motion amount to a considerable out-of-plane displacement of the acetyl group. For this reason, it is important to check the possible role of this motion in the charge-separation process. In our calculation on the transition state, we modeled this motion by varying the angle corresponding to acetyl out-of-plane motion. We believe that simulation of the rocking motion of the macrocycle and tilting of ring I will give the same result. As we will see below, the reason the motion of the acetyl group couples to charge separation is that the negatively charged oxygen is situated between P_A and B_A and therefore affects strongly the orbitals involved in the charge separation. For this reason, it is also important to take into consideration the mode at 137 cm^{-1} that contains a great contribution from in-plane motion of the acetyl group.

The full analysis of low-frequency vibrations will be given elsewhere. It is important here to consider the question concerning the correspondence between the calculated and experimental

TABLE 1: Calculated Vibrational Spectra Compared to RR Spectra^{26,30,31} and Oscillations in the B_A²¹ and B_A⁻²³ Absorption Spectra Due to Coherent Nuclear Motions

Models			description for the 82 atoms (+ heavy atom) model ^a	RR		Osc
55 atoms ^b	70 atoms ^b	82 atoms + heavy atom ^b		P ^b	BCl _{LM} ^b	
24	21	6	roc BCl (ring II, IV), tor (Im)	36		12
		13	roc BCl (ring I, III), δ MgIm			
		21	γ (COCH ₃) _{2a} , δ CH ₃ (OCOCH ₃) ₁₀			
		26	δ (OCOCH ₃) ₁₀ , δ (CH ₃) _{3a,4a} , γ (CH ₃) _{1a,5a}			
31	31	27	tor (Im)	36		30
		32	swivel (ring II, III, IV, I), δ (CH ₃) _{3a,4a,7a,8a}			
		36	swivel (ring II), tilt (ring IV), δ (CH ₃) _{3a,8a,4a,7a}			
35	27	38	tor (COCH ₃) _{2a} , γ (CH ₃) _{1a} , δ (CH ₃) _{3a,4a}	72	56	
		41	tor (OCOCH ₃) ₁₀			
47	47	48	swivel (ring III, IV, V), δ (CH ₃) _{3a,4a,7a,8a}	96	87	
58	49	55	transl (ring I, III), γ C ₉ O, δ (OCOCH ₃) ₁₀			
60	57	60	swivel (ring I, III), tor (CH ₃) _{1a}	130	118	130
			γ C ₁ (CH ₃) _{1a} , γ CO(COCH ₃) _{2a}			
		76	γ C ₁ (CH ₃) _{1a,5a} , γ CO(COCH ₃) _{2a} , transl (ring V)			
		84	tor (CH ₃) _{5a}			
91	87	79	γ (CH ₃) _{5a} , γ C ₉ O, γ CN (rings III, IV)	137 (2) {2}	137 (1) {2}	
		91	γ CN (rings I, II), γ C _m H, tor (CH ₃) _{5a} , δ (CH ₃) _{3a}			
		93	tor (CH ₃) _{5a} , γ CN(rings I–IV), γ C ₁ (CH ₃) _{1a}			
		118 (0.1) {0.5}	δ MgIm, γ Mg _{dome} , γ C ₉ O			
126	111	119	tor (CH ₃) _{1a} , γ Im, γ CN (ring I–IV)	143[2]	137[2]	
		127	δ (COCH ₃) _{2a} , δ (CH ₃) _{3a,4a,7a,8a} , γ CN, γ C ₉ O, γ CH			
		131	δ (CH ₃) _{3a,4a,7a} , γ (CH ₃) _{5a} , δ (COCH ₃) _{2a}			
		141	tor CH ₃ (OCOCH ₃) ₁₀			
141	143	133	tor (CH ₃) _{1a} , γ CO(COCH ₃) _{2a}	144	163	
169 (1.2) [1.4]	150[0.8]	151[1.1]	γ CN (rings I–IV), γ C ₁ (CH ₃) _{1a}			
			δ (CH ₃) _{3a,4a,7a,8a}			
		157 [0.4]	tor CH ₃ (OCOCH ₃) ₁₀ , δ C ₉ O,			
173	158	164	δ/γ CNC, δ/γ CCC	179 (2) [1]	190 (2) [2]	
			δ (CH ₃) _{3a,4a,7a,8a,5a} , δ C ₉ O,			
			δ/γ CNC, δ/γ CCC			
		166 [0.6]	δ (CH ₃) _{3a,4a,7a,8a} , γ CN (ring I–IV)			
228 (1.9) [1.4]	182 (3)	175	δ (CH ₃) _{3a,4a,5a,7a,8a} , δ/γ CNC, δ/γ CCC	203 [2]	185 [1]	
		234 (1.4) [0.7]	tor (CH ₃) _{2b} , γ Mg _{dome} , γ CN (ring I,II),			
			tor (CH ₃) _{3a,4a,7a,8a}			
		186	δ (CH ₃) _{3a,4a,5a,7a,8a} , δ/γ CNC (ring I)			
181 (0.2) [0.9]	188 (0.3)	196	δ (CH ₃) _{5a} , δ C ₉ O, δ CNC, δ CCC	240	220	
207	197	209 [0.7]	macrocycle breathing, δ (CH ₃) _{3a,4a,7a,8a} ,			
190 [0.7]	210 [0.7]		tor (CH ₃) _{2b}			
		221 [0.4]	tor (CH ₃) _{3a,4a,7a,8a,2b} , γ CN (ring I–IV), δ (CH ₃) _{5a}			
236 (1.4) [1.2]	230	217 [0.6]	tor (CH ₃) _{2b} , γ Mg _{dome} , γ CN (ring I–IV)	236 (<1) {<2}	240 (1) {<2}	
241 [0.7]	222 [1]	238 (0.5)	tor (CH ₃) _{3a,4a,7a,8a} , γ Mg _{dome} ,			
233 [1.5]	233		γ CNC (ring I)			
		240	tor (CH ₃) _{3a,4a,7a} , γ Mg _{dome} ,			
	240	240	γ CN (ring II, IV)	240	220	
	251	244 (0.7)	tor (CH ₃) _{3a,4a} , γ Mg _{dome} ,			
			γ CNC (ring II, IV)			
	248	245	tor (CH ₃) _{3a,4a,7a}			
	242	248	tor (CH ₃) _{3a,4a,8a}	236 (<1) {<2}	240 (1) {<2}	
	252	250	tor (CH ₃) _{3a,4a,7a,8a}			
	256	256 (0.7) {0.2}	tor (CH ₃) _{3a,4a,7a,8a} , γ Mg _{dome} , γ Im			
		261 (0.1) {1}	γ Im, tor (CH ₃) _{7a,8a,10a} , γ Mg _{dome}			

^a Mode descriptions are as follows: ν = stretch, δ = bending, γ = out-of-plane (for macrocycle or imidazole) deformation, tor = torsion, roc = rocking motion (see text for comments). For a description of tilt, swivel, and translation, see ref 51. ^b Calculated (²⁶Mg), [¹⁵N] for BCl, and {¹⁵N} for imidazole (only for N connected to Mg) isotope shifts.

isotope shifts. As can be seen from Table 1, there is a quite satisfactory agreement between theory and experiment, except for one of the shifts calculated for the mode at 118 cm⁻¹, which we assign to the RR line at 137 cm⁻¹. The calculated wavenumber varies on ¹⁴N–¹⁵N substitution on the imidazole nitrogen bonded to the Mg atom of BChl *a*, but somewhat less than in the experiments.

Experimentally, the RR lines at 137 and 180 cm⁻¹ are sensitive to Mg isotope substitution. On the basis of our calculations it is most reasonable to assign the line at 180 cm⁻¹ to Mg out-of-plane dome motion, because the latter mode is sensitive also to ¹⁴N–¹⁵N substitution of the macrocycle N atoms

involved in this motion. The 137 cm⁻¹ mode, on the other hand, is sensitive to ¹⁴N–¹⁵N substitution of the axial imidazole, because of a considerable contribution of bending motion of the imidazole along the line connecting the nitrogen atoms of rings I and III.

It will be important for the forthcoming discussions to know the width of the vibrational wave function as a function of wavenumber. The torsional Schrödinger equation is given by

$$-\frac{\hbar^2}{2I} \frac{\partial^2 \Psi}{\partial \theta^2} + \frac{\omega^2 I}{2} \theta^2 \Psi = E \Psi \quad (2)$$

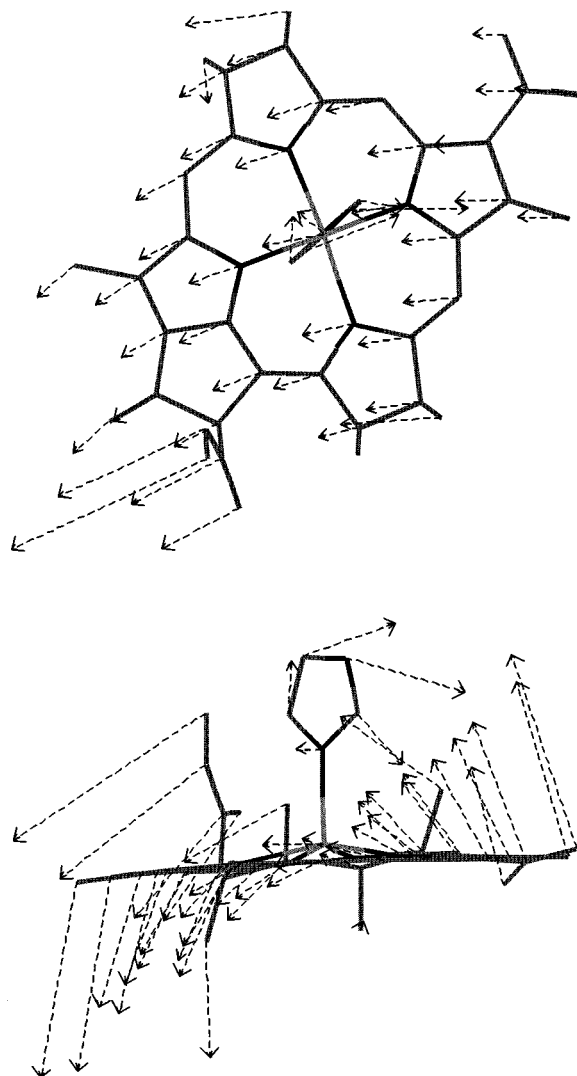


Figure 7. Rocking vibrational mode of the BChl *a* macrocycle at 13 cm^{-1} for the 82-atom model. An atomic mass of 200 has been introduced on the hydrogen atom bonding to the imidazole carbon atom farthest away from the Mg atom.

The moment of inertia is I and the vibrational frequency $\nu = \omega/(2\pi)$. The measured wavenumber is $\omega/(2\pi c)$, where c is the velocity of light in centimeters per second. If we write the ground-state wave function as $\Psi = \exp(-\alpha\theta^2)$, the width of the density ψ^2 at half-maximum is $2\theta_{1/2} = (2 \ln(2)/\alpha)^{1/2}$. If this expression for the wave function is inserted in eq 1, we obtain $\alpha = I\omega/(2\hbar)$ and hence

$$\text{width} = 2\theta_{1/2} = \left(\frac{\hbar \ln 2}{I\omega} \right)^{1/2} \quad (3)$$

For example, the acetyl group of ring I has width $2\theta_{1/2} = 20^\circ$ in the lowest vibrational state.

4. Electronic Structure and Spectra of Reaction Center

Previous theoretical work on the special pair has involved calculations of semiempirical^{11–13,33,52} and ab initio type^{14,15,34,37} of the electronic spectrum. Self-consistent reaction field calculations on the special pair of *Rhodopseudomonas* (*Rps.*) *viridis* indicated a great red shift of the absorption energy,³³ thus explaining the large experimental red shift as a combination of exciton splitting and charge separation within the special pair. This indicates that the S_1 state of P has character of both local

TABLE 2: Sensitivity Test for S_1 State for BChl Monomer (P_B), Special Pair ($P_B + P_A$) and Special Pair Plus One Accessory BChl ($P + B_A$) for *Rb. Sphaeroides* (ZINDO/S Calculation)^a

simulated mode	$(\Delta\nu/\nu) \times 10^4$				
	P_B	$P_B + P_A$	$P_B + P_A + B_A$ CT- S_1 split 6446 cm^{-1}	$P_B + P_A + B_A$ CT- S_1 split 180 cm^{-1}	$P_B + P_A + B_A$ CT- S_1 split 45.7 cm^{-1}
out-of-plane	1.0	60			
torsion	1.5	26	19	18.8	21.9
in-plane bending	4.3	30			

^a The dihedral angle or the out-of-plane or in-plane bending angles of the acetyl group of ring I are changed by 1.06° , causing a change of the absorption wavenumber of the S_1 state (ν) equal to $\Delta\nu$.

excitation and charge transfer. Similar mixing is expected for the reaction center of *Rb. sphaeroides*. Recent DFT calculations have focused on geometry optimization, vibrational levels, and charge distribution in the positive ion of the special pair.^{34,36–41}

We have carried out a number of calculations on the locally excited and charge-transfer states of the special pair (P) using the ZINDO/S method^{47,52} and found that energies as well as transition moments of the excited states are sensitive to the nuclear positions of the side groups, as has been previously described by Fajer et al.²⁵ Because we will later simulate the reaction field by introducing charges in the environment of the chromophores that bring the lowest charge-transfer state, of type $P^+B_A^-$, close in energy to the locally excited S_1 state, we also calculated the sensitivity in the presence of the latter charges. In Table 2, we see that nuclear motions probably involved in some of the low-energy RR lines^{30,31} also affect the position of the excited states. This measure of sensitivity has been calculated for the motion of the acetyl group of ring I. We see that the sensitivity is much greater in the dimer P than in the monomer (Table 2). The sensitivity is about the same as without reaction field.

Generally, the greater the sensitivity the more prominent are the oscillatory features of the emission. At the same time, it is likely that the greater the sensitivity, the greater is the change in equilibrium geometry between ground and excited state. The intensities of the RR lines, in their turn, are directly dependent on the magnitude of the change of equilibrium geometry.⁵³ The greater sensitivity (Table 2) to nuclear motions thus explains why the RR lines at low energy are relatively stronger for the dimer P than for the monomer BChl.^{30,31} The great sensitivity of the PES to the side-group motions of P depends on partial charge-transfer character of the $S_0 \rightarrow S_1$ excitation. Charge-transfer involves changed occupations of a π orbital, which extends to some side groups, in particular the acetyl group of ring I.

The strong involvement of the side groups in the low-frequency dynamics is consistent with the fact that different RCs with the same special pair and accessory BChl on the A side have very similar spectra.²² Apparently, the structure of the surrounding protein is less important than side-group motion. The reason is simply that side-group motion but not protein motion is affected by occupation number changes in the π -systems.

Oscillations in stimulated and spontaneous emission^{16–24} may also be caused by dependence in the oscillator strength on the side-group positions. The S_1 state is composed of locally excited and charge-transfer components.^{33,34} The mixing coefficients are strongly dependent on the position of the side groups.

In a calculation on P, we find that the LUMO of P_B has a lower energy than the LUMO of P_A . The main reason is that

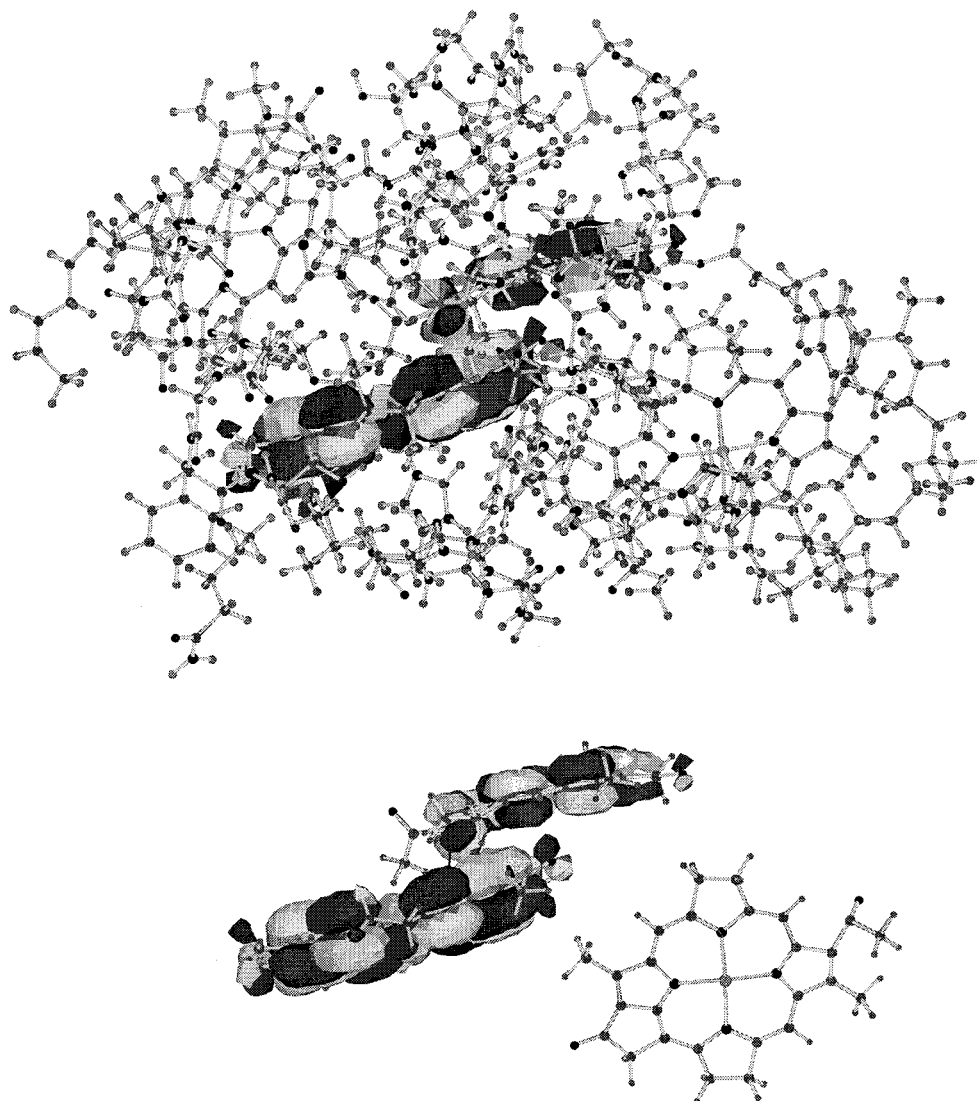


Figure 8. Atoms included in the large and small calculation of the spectrum using the ZINDO/S method.⁵³ The LUMO is shown.

the former MO is π -bonding with the acetyl group of ring I. The same energy lowering is not obtained by the LUMO on P_A because the acetyl group is involved in hydrogen bonding and almost perpendicular to the plane of the macrocycle. We thus expect that the wave packet on the S_1 surface of P immediately after excitation moves toward P_B . Charge migration of this type may also be caused by a reaction field, but it has turned out to be difficult to single out any structural features in the protein as a cause of such charge transfer within P.

Two calculations were done of the spectrum of $P + B_A + B_B$. In one, we included the truncated structures of Figure 2a and in the other a large part of the surrounding protein (Figure 8). The ZINDO/S calculation gave a transition wavelength for the lowest transition at 951 nm in the small calculation and 1035 nm in the large calculation. These values are a little too high. One expects a larger value for the larger system because part of the reaction field is effectively included in the large calculation. The ZINDO/S method apparently predicts too small excitation energies for the special pair because the agreement with the experimental spectrum is acceptable without reaction field. Figure 8 also shows that the LUMO looks the same in both calculations, indicating that the character of the excited state depends mainly on the local macrocycle structure.

5. Charge Separation Depends on the Position of the Acetyl Group of Ring I

We have seen above that a wave packet is formed mainly on P_B shortly after excitation, which means that the geometry changes accompanying the formation of the charge-separated state are localized on the P_B part of the special pair and correspond mainly to differences between the neutral system and the negative ion of a single BChl *a*. This means that activation of a number of low-frequency modes are coupled to charge separation. We will show that the acetyl group of ring I is particularly involved and that simulation of its motion leads to great changes in the electronic density distribution.

There is experimental and theoretical evidence that the primary charge separation is activation-less. In fact, the rate of charge separation in the wild-type RC decreases as the temperature is increased,³⁵ while for several mutants there is an increase of rate with temperature. The vanishing activation energy is consistent with the small calculated reorganization energy and the fact that the charge-separated $P^+B_A^-$ state is slightly lower in energy than the P^*B_A state. Important evidence for this is provided in a recent paper by Spörlein et al., who find that pigment replacement of B_A by a pigment with a slightly higher energy of the charge-separated state leads to a much lower ET rate.⁵⁵

TABLE 3: Study of the Transition State for Photoinduced ET between P and B_A for the Reaction Center of *Rb. Sphaeroides*^a

separation ^b (cm ⁻¹)	contribution of P ⁺ B _A ⁻ to the lowest state (%)	oscillator strengths for upper/lower state	Δθ ^c	Δ ^d (cm ⁻¹)
558	99.8	0.76/0.0005	-18.1	6.5
97	96.9	0.72/0.02	-2.9	27.9
59	92.2	0.65/0.06	-1.6	29.7
45.7	86.0	0.63/0.1	-1.1	30.4

^a The torsion angle of the acetyl group of ring I of P is varied (ZINDO/S calculation). ^b Original separation in cm⁻¹ between the CI states formed from P*B_A and P⁺B_A⁻. ^c Change of dihedral angle of acetyl group of ring I of P_B necessary to reach transition state. Negative value is used if the state with mainly P⁺B_A⁻ is lower before turn. ^d Separation between CI states after change of angle.

Accurate calculation of the relative position of the locally excited and charge-separated PES is not possible at the present. Very rough calculations assuming polarization fields described by Born spheres with a single dielectric constant are possible and lead to reasonable results, showing that the basic theoretical model is qualitatively correct.^{12,39} Quantitative data cannot be provided in such calculations because a dielectric constant has to be chosen more or less arbitrarily. Better ways include all charges and dipoles of the protein as accurately as possible. Such calculations have been carried out by Parson et al.⁵⁶ and suggest that the energy of the P⁺B_A⁻ state is about the same as that of the P*B_A state in *Rps. viridis*. Of particular importance to us is that tyrosine M208 (M210 in *Rb. sphaeroides*) was found to play an important role in lowering the energy of the P⁺B_A⁻ state.⁵⁶

To simplify the present study, we decided to empirically fix the relative positions of the P⁺B_A⁻ state and the P*B_A state on the energy scale, roughly as suggested in refs 23 and 55 with use of point charges. These charges were chosen to give an energy separation between the charge-separated P⁺B_A⁻ state and locally excited P*B varying from -500 to 500 cm⁻¹. For each chosen value, the torsion angle and other angles of the acetyl group of ring I are varied to simulate motion in the transition-state region. These calculations were done using the semiempirical ZINDO/S model⁵³ and include P and B_A.

Some results are summarized in Table 3. The first line shows that at a wavenumber difference of 558 cm⁻¹ the first excited singlet state has 99.8% charge-transfer character of type P⁺B_A⁻, with the electron on the accessory B_A. The small oscillator strength (0.0005) is borrowed from the small locally excited component of this state. A torsion angle of -18.1° is necessary to reach the transition state, where the wave function has half P*B_A and half P⁺B_A⁻ character. The minus sign indicates that the torsion angle must be turned in a direction that corresponds to reverted ET. At a difference of 45.7 cm⁻¹, we need to turn back only 1.1°. Naturally, if the P⁺B_A⁻ state is close in energy to the locally excited P*B_A, less change is needed to achieve the transition state. The results in Table 3 show that the charge distribution is very sensitive to change of dihedral angle at a geometry that is close to the ground-state geometry. If the torsion angle had not been important for ET, it would not have been possible to achieve the transition state by changing the torsion angle at all, for a reasonable energy difference between the states.

In Table 4, the angles for out-of-plane motion, torsion, and in-plane bending have been changed in the vicinity of the transition state. We see that the charge distribution is very sensitive not only to the torsional motion but also to the other

TABLE 4: Study of the Transition State for Photoinduced ET between P and B_A for the RC of *Rb. Sphaeroides* Using ZINDO/S Calculation^a

simulated motion	angle CT lower ^b	angle CT higher ^c	Δ (cm ⁻¹) CT lower ^b	Δ (cm ⁻¹) CT higher ^c
out-of-plane	-0.9	1.3	30.5	33.3
torsion	-1.1	1.0	30.4	33
in-plane bending	-5.0	3.3	30.3	32.4

^a The P*B_A and P⁺B_A⁻ are fixed at an energy difference corresponding to ±45.7 cm⁻¹. Out-of-plane, torsional, and in-plane angles of the acetyl group of P_B are varied to reach the transition state. ^b Refers to the case when the lowest state is of type P⁺B_A⁻ with 45.7 cm⁻¹ difference. ^c Refers to the case when the highest state is of type P⁺B_A⁻ with 45.7 cm⁻¹ difference.

TABLE 5: Study of the Transition State (TS) for Photoinduced ET between P and B_B for the RC of *Rb. Sphaeroides* Using ZINDO/S Calculation^a

simulated motion	angle	Δ (cm ⁻¹)
out-of-plane	TS not achieved	TS not achieved
torsion	-11.8	8.8
in-plane bending	1.6	11.3

^a The P*B_B and P⁺B_B⁻ are fixed at an energy difference corresponding to the latter state being lower by 45.7 cm⁻¹. Out-of-plane, torsional, and in-plane angles of the acetyl group of P_A are varied to reach the transition state.

angles. The transition state may be reached with only small modifications. The ET coupling, which is half the state energy difference, Δ, at the transition state, is close to 15 cm⁻¹ in all cases. In earlier papers,^{12,13} we have used two different methods to reach the transition state: mixing of states and mixing of orbitals. We now obtain nearly the same result by these two methods.

In Table 5, we present the results when the corresponding geometry modifications for charge separation on the B-side are carried out. In this case, we modify the angles of the P_A acetyl group and consider the transition state for P*B_A → P⁺B_B⁻. We find less sensitivity of the charge distribution to the change of angle. Only for in-plane bending, corresponding to the 130 cm⁻¹ wavenumber, it is possible to obtain the transition state for a small change of angle. The coupling is only one-third of the coupling on the A-side.

As an experiment to further study the sensitivity of the charge distribution, we replaced the acetyl group by vinyl or formyl groups. Of the latter, only the formyl group was cooperative in charge separation but less effectively so than the acetyl group. The electronic coupling between P_B and B_A was much less with the vinyl group but only slightly less with a formyl group. This result suggests that it is mainly the oscillating charges of the acetyl group that are capable of modifying the relative energies of the local LUMOs, thereby affecting the total charge in the direction of charge separation.

In addition to side-group oscillations, the high-frequency CC and CN stretch vibrations are capable of inducing charge separation. At least one of these modes must be involved to accomplish ET between two locations. If two modes are necessary for the P⁺B_A⁻ state to be stable, the one with the lowest frequency determines the initial rate of the wave packet, if the latter starts out in the locally excited equilibrium geometry. On the other hand, it is easy to see that if the high-energy mode is the only one necessary to reach a stable P⁺B_A⁻ state, this mode is also the only activating mode and consequently the rate is correspondingly higher. If both modes are present and necessary for the activation, one may use the average mode frequency.⁵⁷

$$v_n = \frac{\sum_i v_i^2 \lambda_i}{\sum_i v_i \lambda_i} \quad (4)$$

The wave packet is formed corresponding to the ground state, which is close to the left minimum because the reorganization energy is small for excitation to the locally excited state P*B. The wave packet follows a PES where the major component of the wave function is P*B, goes through a saddle point corresponding to the activated state, and enters a region where the major component of the wave function is charge-separated P⁺B[−]. Equation 4 gives the rate at the top of the barrier. In the beginning and end of the reaction path, the wave packet moves, however, with a much lower rate because it is the slow side-group motion that sets the rate.

In the next section, we will try to determine the rate for the case with equal free energy of P*B and P⁺B[−] states. Obviously, the first vibrational level at about 1500 cm^{−1} is well above the PES barrier, equal to or less than $\lambda/4 \cong 0.04$ eV = 320 cm^{−1}. Hence, one should use a coherent model for wave packet motion.

6. Discussion of Rate

A vibrational model for ET in the case of small or absent activation barrier has been set up in earlier work.⁴³ The rate is obtained by including the corrections to the Born–Oppenheimer approximation of the nonintersecting potential energy surfaces (PESs) of the Marcus model in a variational calculation, where the basis functions are harmonic functions. In the limit of large coupling, the rate of ET is determined by the vibrational frequency, as in the original Marcus rate model. On the other hand, if the coupling tends to zero, the rate is proportional to $|\Delta|$ if the acceptor state is immediately depleted, as appears to be the case for the RC (the Rabi rate⁵⁸).

The Marcus–Sutin model for ET⁹ should not be applied in the case when there are less than a few vibrational levels below the ET barrier and particularly when there is no activation barrier at all. In such a case, the above-mentioned model⁴³ or the vibrational model of Jortner et al.^{10,59} may be used. With use of the former model,⁴³ it turns out that even if the activation energy is absent, the shape of the adiabatic ground-state PES affects the rate. If the ET coupling is large, the maximum possible rate is set by the fastest mode coupled to ET, for example, a CC stretch frequency. The CH stretch mode is not connected to any reorganization energy and is in most cases inactive in bringing about charge separation. Therefore, the CC stretch mode sets the rate of the wave packet if Δ is large. A value of 1600 cm^{−1} corresponds to $\tau = 20$ fs. However, because Δ is small, the rate is usually much lower. If we assume that $\Delta = 30$ cm^{−1}, reorganization energy $\lambda = 0.15$ eV, vibrational frequency $\tilde{\nu} = 1500$ cm^{−1}, and effective mass = 6 amu, the calculated energy splitting, using the model of ref 43, is about 100 cm^{−1}, which corresponds to a time constant of about 0.3 ps. This is a factor of 7 faster than the measured one. On the other hand, if only the low-frequency modes are involved ($\tilde{\nu} = 30$ cm^{−1}), we obtain a rate rather close to the experimental one (2 ps). Summarizing, we find that the rate of charge separation is not particularly large in bacterial photosynthesis in comparison to the maximum possible rate but apparently fast enough to effectively compete with waste processes, such as fluorescence or triplet formation.

The incoherent rate for the two wild-type RCs has previously been calculated by Fleming et al.³⁵ using the vibrational model

of Jortner and Bixon,^{10,59} assuming a single mode and by Klevanik.⁶⁰ This model gives good agreement with the experimental rate as a function of temperature, if $V = 24$ cm^{−1} is assumed, a value rather close to $V = 30/2 = 15$ cm^{−1} obtained here. For *Rps. viridis*, it was not possible to obtain good agreement with the experimental curve in the whole temperature range. However, a slightly larger value of V gives a good agreement except for temperatures close to room temperature, where a somewhat too large rate is predicted. Because of the complexity of the problem, there are many possibilities that may explain this disagreement. Simplified theoretical models cannot be expected to hold precisely in all cases.

The difficulty with rate calculation in the present case is that the high-frequency mode is connected to appreciable reorganization energy but less well suited for coherent wave packet formation and motion because the vibrational energy is much larger than the accessible energy. The low-frequency modes, on the other hand, are almost classical and useful for wave packet motion. Provided that the energy of the intermediate P⁺B[−] state is sufficiently low, these modes can transfer the excited electron at a rate that is still sufficiently high as a charge-separation mechanism.

7. Discussion of Mechanism, Wild Type

We have been able to identify a number of nuclear modes in the low-frequency region, some of which are clearly coupled to the primary charge-separation process in bacterial photosynthesis. The identification is based on the fluctuation in the charge distribution during the vibrational cycle.

The calculated low-energy modes have frequencies similar to the oscillatory features seen in the stimulated and spontaneous emission spectra in the region of P* by Vos et al.^{16–18} and Stanley and Boxer,¹⁹ respectively, and in the absorption spectrum in the region of B_A[−] by Streltsov et al.^{20,21} Our results are also consistent with the results of Spörlein et al.,²² Yakovlev et al.,²³ and Vos et al.²⁴ The latter have criticized the conclusions of Streltsov et al.^{20,21} on the grounds that the lifetime of the P⁺B_A[−] state is too short to connect the oscillations to formation of the latter state. However, both the results of Streltsov et al., which demonstrate a correlation between ET rate and intensity of the low-frequency oscillations, and those of Vos et al., who show a correlation with an electrochromic shift,²⁴ point to involvement of the slow modes in the ET process. Spörlein et al. favor a different model to explain the oscillations.²²

The oscillations identified here are primarily due to side-group motions. We find that ET is coupled to out-of-plane, torsional, and in-plane oscillations of the acetyl side group of ring I of the special pair and possibly the side groups of B_A and Φ_A . These frequencies are modified to some extent by the surrounding protein. In particular, attachment of the axial imidazole to the protein leads to intermacrocycle motions of the special pair. The latter motion may also be active in charge separation.

Vos et al. have pointed out that there may be phase coherence between the primary charge separation and the continued ET from B_A to Φ_A . Our results support this conclusion. High probability for an ET process occurs when the turning point on the PES, corresponding to charge transfer, is on the same vertical as the ground-state equilibrium. One may even suggest that there is evolutionary pressure to achieve such optimum conditions for wave packet motion. The fluctuations around the equilibrium increase as the temperature is increased, and consequently, if the mentioned optimum arrangement of PES has been achieved, the rate should increase as the temperature is lowered. This has been found to be the case for both *Rps. viridis* and *Rb*.

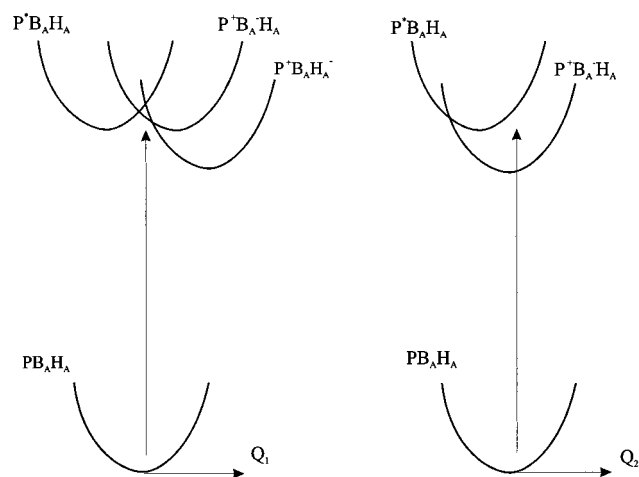


Figure 9. Model projected PES for the modes at 30 cm^{-1} (left) and 13 cm^{-1} (right).

sphaeroides.³⁵ On the other hand, the rate decreases normally at increased T in barrierless ET.^{10,35,59} In Figure 9, we have tried to outline the position of the diabatic energy surfaces on the basis of our calculations for the two most important modes. The cycle time corresponds closely to the measured charge-separation rate.

Previously, the protein modes have been considered as more important than the side group modes by most investigators. Although, for example, the phenol group of M210 may be important, protein modes in general appear to be less likely to have a role in charge separation because the region around the special pair is known to be nonpolar. This nonpolar nature of the protein is important to keep the contribution from the protein to the reorganization energy low.

It has been suggested that some of the modes seen in RR spectra are involved in charge separation.^{29–31} Our results give credibility to the suggestion that the equilibrium geometry is dependent on occupancy of orbitals, which is changed at excitation and consequently gives intensity to the RR lines.⁵⁴

The energy of the $\text{P}^+\text{B}_\text{A}^-$ state is of crucial importance. If it is above the energy of the $\text{P}^*\text{B}_\text{A}$ state, the rate decreases by a factor of 10 for each 500 cm^{-1} above because of the Boltzmann factor. On the other hand, in the sequential model, the rate of back reaction to the locally excited triplet state ($\text{P}^+\text{B}_\text{A}\Phi^- \rightarrow {}^3\text{P}^*\text{B}_\text{A}\Phi_\text{A}$) also decreases by a factor of 10, as discussed in the Introduction. Consequently, if the energy of the $\text{P}^+\text{B}_\text{A}^-$ state is low, charge separation can compete effectively with excitation back to the antenna system,⁶¹ fluorescence, and other wasteful processes. It must not be too low because then the rate of back reaction to the triplet state would increase.

The involvement of the side groups in ET in fact limits the ET rate to the cycle time of the low-frequency modes. A possible useful role of the side groups is to localize the wave packet and make it move as a classical “particle”, thereby avoiding delocalized charge separation. A related interesting question is why the charge separation has not evolved a structure with a very large electronic coupling to increase the rate even further. Except for the obvious answer that such an increase would not be of any interest because the rate is already sufficiently high to compete with other decay mechanisms, it is also true that a too large electronic coupling would not permit complete charge separation, that is, localization on a single cofactor molecule. This question is related to the problem of the best conditions for depletion of the wave function to the next cofactor in the chain. We refer to a paper by Reimers and Hush.⁵⁸

TABLE 6: Energy of Charge-Separated State in ZINDO/S Calculations Compared to Measured Charge-Separation Rates^a

modeling side group of residue	calculated $\text{P} \rightarrow \text{B}_\text{A}$ transition		difference to WT (cm^{-1})	measured time constant for $\text{P}^*\text{H}_\text{L} \rightarrow \text{P}^+\text{H}_\text{L}^-$ (ps)	
	nm	cm^{-1}		295 K	80 K
Tyr ^b	658	15 195	0	3.5 ± 0.3^c	1.7 ± 0.2
Tyr ^d	612	16 337	1142		
His ^b	677	14 775	−419	3.7 ± 0.4^c	2.6 ± 0.2
His ^d	591	16 924	1729		
Phe	632	15 822	628	10.5 ± 1.0^e	10.5 ± 1.0
Ile	630	15 877	682	16 ± 2^e	55 ± 5
^f	629	15 904	709		
Trp	616	16 233	1039	41.4 ± 4^e	155 ± 10

^a Average of two calculations are taken where either the structure of wild type or the structure of the YM210W mutation is kept, while in both cases the side group of M210 (M208) is replaced by the side groups of natural or mutated residues. ^b H of OH or NH groups for tyrosine or histidine directed to B_A , corresponding to amino acid dipole moment orientation preferable for the CT state stabilization. ^c Reference 63. ^d H of OH or NH groups for tyrosine or histidine directed toward P (opposite to case footnote b). ^e Reference 66. ^f No side group included.

8. Discussion of Mutants

We converge on a model for bacterial charge separation that may be tested in applications on *Rps. viridis* and other species as well as mutated species. In *Rps. viridis*, the special pair is bonded to the protein in a slightly different way than in *Rb. sphaeroides*. The tyrosine M208 side group (M210 in *Rb. sphaeroides*), however, is conserved, as it also is in *Rhodospirillum rubrum*, the first systems in which the intermediate state was discovered.² The phenol group of this residue points into the region between P and B_A . Chan et al. studied mutants of *Rb. capsulatus* and found differences in charge-separation rates when M208 is mutated.^{62,63} The only mutant that has a higher rate than wild type is YM208H.

One particularly well-studied mutant is YM210W, which has a much slower ET rate than wild-type *Rb. sphaeroides*. Streltsov et al.^{20,21} found that the oscillations are weaker in this RC, which can be directly related to the lower rate of ET. The structure of this mutant has been determined and found to be very similar to that of wild type.⁶⁴ The most reasonable explanation for the low ET rate is that the energy of the $\text{P}^+\text{B}_\text{A}^-\Phi$ state is higher in the mutant than in the wild type.^{65,66} As pointed out by Finkel et al. before the structure was known, various spectroscopic methods suggest that there is probably no great structural difference between wild type and the mutant and that the great difference in rate has to do with the molecular properties of the tyrosine and tryptophan side groups.⁶⁵

To examine the problem of the relative energy of the $\text{P}^+\text{B}_\text{A}^-$ state in wild type and mutant, we replaced tryptophan by tyrosine and other mutants in the crystallographic data for the YM210W mutant⁶⁴ but kept exactly the same structure for P and B_A . The same position was used for peptide and C_β . Single-point calculations using B3LYP with a 6-31G* basis were performed. It was found that the proton of the tyrosine hydroxide group in the ground state points in a way that leads to low energy of the $\text{P}^+\text{B}_\text{A}^-$ state. Subsequently, we performed a ZINDO/S calculation in a simulated reaction field. We found that the $\text{P}^+\text{B}_\text{A}^-$ state is about 1000 cm^{-1} lower in wild type than in the mutant. In another ZINDO/S calculation including P, B_A , and B_B , we found that the mutant has the same energy for the $\text{P}^+\text{B}_\text{B}^-$ state as for the $\text{P}^+\text{B}_\text{A}^-$ state, whereas the energy for the $\text{P}^+\text{B}_\text{B}^-$ state in the wild type is considerably higher than that for the $\text{P}^+\text{B}_\text{A}^-$ state (Table 6). These results are consistent with results from molecular dynamics calculations.^{42,56,67}

In a follow-up calculation, we used the structure of the wild type but replaced tyrosine by tryptophan. Almost the same result was obtained as previously when we used the structure of YM210W but replaced tryptophan with tyrosine. The same procedure was performed for the mutants of *Rb. capsulatis*. The two calculations, changing only M208 for another residue in two possible crystallographic structures, gave about the same result. In Table 6, we give the average of the two calculations. As we see, the higher the energy of the $P^+B_A^-$ state, the lower is the charge-separation rate.

Rischel et al.⁶⁸ have studied mutations with the purpose of understanding the functional role of the oscillations. They find that the mode energies are much changed for certain mutations, for example, when hydrogen bonds are manipulated. They conclude that the protein is playing a major role. This goes partly against the conclusions in refs 29 and 30. Our results show that attachment of the cofactors to the protein, for example, by hydrogen bonds, does change the character and energies of the modes to a considerable extent. Furthermore, the intensity may be affected depending on whether charge transfer is coupled to the mode, as we have seen above. Still our conclusion is that it is the cofactor part of the mode that is of importance for charge-transfer rather than the protein part. Our results are therefore consistent with both models mentioned above.^{29,30,68}

Possibly a contribution to rate differences comes from differences in electronic coupling between P and B_A . We found indeed a somewhat smaller coupling, about 60% of wild type, in the YM210W mutant.

Van Brederode et al.^{69,70} found that excitation in the absorption band of B_A leads to very fast charge separation without involvement of P^* . This strongly suggests that the coupling, which here involves HOMO and HOMO-1, is quite large. The reason for the fast charge separation at excitation of the accessory chromophore of the mutant is very likely that the PB_A^* state (but not the P^*B_A state) is higher in energy but with a similar equilibrium geometry as the $P^+B_A^-$ state. The higher energy of the precursor state is sufficient to avoid an unfavorable Boltzmann factor. The higher rate may have to do with the different shape of the energy curve when the free energy of the reaction is large. According to our discussion above, there are some possibilities to get a faster rate than in the natural system. We conclude that it is possible to explain the experimental rate results for wild type and mutant at excitation of both P and B_A within the same theoretical model.

9. Conclusions

Processes in photosynthetic reaction centers have been studied in quantum chemical calculations by solving the time-dependent and time-independent Schrödinger equations for the electrons of the reaction center. Here, we have attempted to solve the vibrational problem for a single BChl molecule attached to the protein as in the natural system. Bocian et al.^{29–31} and others²⁵ proposed that the vibrations of ring I are affecting the locally excited state and are responsible for some of the frequencies seen in RR spectra. We find that some low-energy vibrations, particularly those of ring I side groups, do affect the charge-transfer excited state and therefore very likely are involved in the charge-separation process. These motions also very likely lead to the oscillations in various spectra, as first discovered by Vos et al.^{16–24}

It has long been known that the main function of the special pair is to provide a low-energy S_1 state by exciton coupling and mixing with charge-transfer states within the pair. Detailed calculations make it possible to reveal and understand the finer

details of the working mechanisms of reaction centers. The importance of the accessory BChl is very likely to provide an intermediate that separates special pair donor P and BPh acceptor (Φ_A) spatially so that the direct coupling between the special pair and Φ_A is low. Charge separation and recombination now both have to take place via the accessory chlorophyll. Forward transfer is still fast but charge recombination is considerably slowed because of a Boltzmann factor and cannot take place to any significant extent during the short lifetime of Φ_A^- . This conclusion is supported by the fact that the energy of the $P^+B_A^-$ state was found to be strongly correlated to the rate of electron transfer.

An important conclusion in this paper is that the side groups of the cofactors are mainly responsible for the oscillations seen in electronic spectra and also affect the rate of charge separation and the rate of charge recombination. That this is the case has been hypothesized since oscillations were first discovered.¹⁶ At the same time, many workers in the field have not found enough evidence in support for this conclusion.^{22,68,71} We find that particularly the acetyl group of ring I is implicated because it carries a rather large charge the motion of which is sufficient to affect the position of the moving electron.

Acknowledgment. We are grateful for continuous support from NFR, the Swedish Natural Science Research Council, and for a special grant from Chalmers University of Technology that covered a half-year stay in Sweden for one of us.

References and Notes

- (1) For a review of the early work, see: Dutton, P. L.; Leigh, J. S., Jr.; Prince, R. C.; Tiede, D. M. In *Tunneling in Biological Systems*; Chance, B., Marcus, R. A., DeVault, D., Schrieffer, J. R., Frauenfelder, H., Sutin, N., Eds.; Academic Press: New York, 1979; pp 319–352.
- (2) Shuvalov, V. A.; Klevanik, A. V.; Sharkov, A. V.; Matveetz, Yu. A.; Krukov, P. G. *FEBS Lett.* **1978**, *91*, 135–139. Chekalin, S. V.; Matveetz, Ya. A.; Shkuropatov, A. Ya.; Shuvalov, V. A.; Yartzev, A. P. *FEBS Lett.* **1987**, *216*, 245–248.
- (3) Holzapfel, W.; Finkle, U.; Kaiser, W.; Oesterheld, D.; Scheer, H.; Stiltz, H. U.; Zinth, W. *Chem. Phys. Lett.* **1989**, *160*, 1–7. Dressler, K.; Umlauf, E.; Schmidt, S.; Hamm, P.; Zinth, W.; Buchanan, S.; Michel, H. *Chem. Phys. Lett.* **1991**, *183*, 270.
- (4) Arlt, T.; Schmidt, S.; Kaiser, W.; Lauterwasser, C.; Meyer, M.; Scheer, H.; Zinth, W. *Proc. Natl. Acad. Sci. U.S.A.* **1993**, *90*, 11757. Schmidt, S.; Arlt, T.; Hamm, P.; Huber, H.; Nägele, T.; Wachtveitl, J.; Meyer, M.; Scheer, H.; Zinth, W. *Chem. Phys. Lett.* **1994**, *223*, 116. Zinth, W.; Huppmann, P.; Arlt, T.; Wachtveitl, J. *Philos. Trans. R. Soc. London, Ser. A* **1998**, *356*, 465.
- (5) Shkuropatov, A. Y.; Shuvalov, V. A. *FEBS Lett.* **1993**, *322*, 168. Franken, E. M.; Shkuropatov, A. Y.; Francke, C.; Neerken, S.; Gast, P.; Shuvalov, V. A.; Hoff, A. J.; Aartsma, T. J. *Biochim. Biophys. Acta* **1997**, *1319*, 242. Franken, E. M.; Shkuropatov, A. Y.; Francke, C.; Neerken, S.; Gast, P.; Shuvalov, V. A.; Hoff, A. J.; Aartsma, T. J. *Biochim. Biophys. Acta* **1997**, *1321*, 1. Kennis, J. T. M.; Shkuropatov, A. Y.; Van Stokkum, I. H. M.; Gast, P.; Hoff, A. J.; Shuvalov, V. A.; Aartsma, T. J. *Biochemistry* **1997**, *36*, 1631.
- (6) Huber, H.; Meyer, M.; Scheer, H.; Zinth, W.; Wachtveitl, J. *Photosynth. Res.* **1998**, *55*, 153.
- (7) Deisenhofer, J.; Epp, O.; Miki, K.; Huber, R.; Michel, H. *J. Mol. Biol.* **1984**, *180*, 385. Deisenhofer, J.; Epp, O.; Miki, K.; Huber, R.; Michel, H. *Nature* **1985**, *318*, 618. Michel, H.; Epp, O.; Deisenhofer, J. *EMBO J.* **1986**, *5*, 2445. Chang, C. H.; Tiede, D.; Tang, J.; Smith, U.; Norris, J. R.; Schiffer, M. *FEBS Lett.* **1986**, *205*, 82. Allen, J. P.; Feher, G.; Yeates, T. O.; Rees, D. C.; Deisenhofer, J.; Michel, H. *Proc. Natl. Acad. Sci. U.S.A.* **1986**, *83*, 8589.
- (8) Maroti, P.; Kirmaier, C.; Wraight, C.; Holten, D.; Pearlstein, R. M. *Biochim. Biophys. Acta* **1985**, *810*, 132.
- (9) Marcus, R. A. *Annu. Rev. Phys. Chem.* **1964**, *15*, 155–196. Marcus, R. A.; Sutin, N. *Biochim. Biophys. Acta* **1985**, *811*, 265–322.
- (10) Jortner, J. *J. Am. Chem. Soc.* **1980**, *102*, 6676–6686. Bixon, M.; Jortner, J. *J. Phys. Chem.* **1986**, *90*, 3795–3800.
- (11) Kuhn, H. *Phys. Rev. A* **1986**, *13*, 3409. E. Kitzing, E.; Kuhn, H. *J. Phys. Chem.* **1990**, *94*, 1699. Källebring, B.; Larsson, S. *Chem. Phys. Lett.* **1987**, *138*, 30. Warshel, A.; Parson, W. W. *J. Am. Chem. Soc.* **1987**, *109*, 6143. Parson, W. W.; Warshel, A. *J. Am. Chem. Soc.* **1987**, *109*, 6152. Won, Y.; Friesner, R. A. *Proc. Natl. Acad. Sci. U.S.A.* **1987**, *84*, 5511; J.

- Phys. Chem.* **1988**, 92, 2208; **1988**, 92, 2214. Hanson, L. K.; Fajer, J.; Thompson, M. A.; Zerner, M. C. *J. Am. Chem. Soc.* **1987**, 109, 4728; **1990**, 112, 7828 (Erratum **1991**, 113, 3626). Thompson, M. A.; Zerner, M. C. *J. Am. Chem. Soc.* **1988**, 110, 606.
- (12) Källebring, B.; Larsson, S. Paper VI in Källebring, B. Ph.D. Thesis, Department of Biochemistry and Biophysics, Chalmers University of Technology, Göteborg, Sweden, 1990. Larsson, S.; Broo, A.; Källebring, B.; Volosov, A. *Int. J. Quantum Chem., Quantum Biol. Symp.* **1988**, 15, 1–22. Larsson, S.; Braga, M.; Broo, A.; Källebring, B. *Int. J. Quantum Chem. Quantum Biol. Symp.* **1991**, 18, 99–118.
- (13) Ivashin, N.; Källebring, B.; Larsson, S.; Hansson, Ö. *J. Phys. Chem. B* **1998**, 102, 5017–5022. Larsson, S.; Ivashin, N. V. *J. Appl. Spectrosc.* **1999**, 66, 539–543.
- (14) Zhang, L. Y.; Friesner, R. A. *J. Phys. Chem.* **1995**, 99, 16479. Hasegawa, J.; Ohkawa, K.; Nakatsui, H. *J. Phys. Chem. B* **1998**, 102, 10410. Hasegawa, J.; Nakatsui, H. *J. Phys. Chem. B* **1998**, 102, 10420–10430. Nakatsui, H.; Hasegawa, J.; Ohkawa, K. *Chem. Phys. Lett.* **1998**, 296, 499–504. Kolbasov, D.; Scherz, A. *J. Phys. Chem. B* **2000**, 104, 1802–1809.
- (15) Reimers, J. R.; Hush, N. S. *Chem. Phys.* **1995**, 197, 323. Reimers, J. R.; Hush, N. S. *J. Am. Chem. Soc.* **1995**, 117, 1302. Reimers, J. R.; Hutter, M. C.; Hush, N. S. *Photosynth. Res.* **1998**, 55, 163.
- (16) Vos, M. H.; Lambry, J.-C.; Robles, St. J.; Youvan, D. C.; Breton, J.; J.-L. *Proc. Natl. Acad. Sci. U.S.A.* **1991**, 88, 8885–8889.
- (17) Vos, M. H.; Rappaport, F.; Lambry, J.-C.; Breton, J.; Martin, J.-L. *Nature* **1993**, 363, 320–325.
- (18) Vos, M. H.; Rappaport, F.; Lambry, J.-C.; Breton, J.; Martin, J.-L. *Biochemistry* **1994**, 33, 6750. Vos, M. H.; Jones, M. R.; Breton, J.; Lambry, J.-C.; Martin, J.-L. *Biochemistry* **1996**, 35, 2687–2692.
- (19) Stanley, R. J.; Boxer, S. G. *J. Phys. Chem.* **1995**, 99, 859.
- (20) Streltsov, A. M.; Yakovlev, A. G.; Shkuropatov, A. Y.; Shuvalov, V. A. *FEBS Lett.* **1996**, 383, 129. Streltsov, A. M.; Aartsma, T. J.; Hoff, A. J.; Shuvalov, V. A. *Chem. Phys. Lett.* **1997**, 266, 347.
- (21) Streltsov, A. M.; Vulto, S. I. E.; Shkuropatov, A. Y.; Hoff, A. J.; Aartsma, T. J.; Shuvalov, V. A. *J. Phys. Chem. B* **1998**, 102, 7293–7298.
- (22) Spörlein, S.; Zinth, W.; Wachtveitl, J. *J. Phys. Chem. B* **1998**, 102, 7492–7496.
- (23) Yakovlev, A. G.; Shkuropatov, A. Y.; Shuvalov, V. A. *FEBS Lett.* **2000**, 466, 209–212.
- (24) Vos, M. H.; Rischel, C.; Jones, M. R.; Martin, J.-L. *Biochemistry* **2000**, 39, 8353–8361.
- (25) Gudowska-Nowak, E.; Newton, M. D.; Fajer, J. *J. Phys. Chem.* **1990**, 94, 5795–5801. Fajer, J. *J. Porphyrins Phthalocyanines* **2000**, 4, 382–385. Barkigia, K. M.; Nurco, D. J.; Renner, M. W.; Melamed, D.; Smith, K. M.; Fajer, J. *J. Phys. Chem. B* **1998**, 102, 322–326.
- (26) Cherepy, N. J.; Shreve, A. P.; Moore, L. J.; Franzen, S.; Boxer, S. G.; Mathies, R. A. *J. Phys. Chem.* **1994**, 98, 6023–6029. Cherepy, N. J.; Holzwarth, A. R.; Mathies, R. A. *Biochemistry* **1995**, 34, 5288–5293.
- (27) Cherepy, N. J.; Shreve, A. P.; Moore, L. J.; Boxer, S. G.; Mathies, R. A. *Biochemistry* **1997**, 36, 8559–8566.
- (28) Cherepy, N. J.; Shreve, A. P.; Moore, L. J.; Boxer, S. G.; Mathies, R. A. *J. Phys. B* **1997**, 101, 3250–3260.
- (29) Palaniappan, V.; Aldema, M. A.; Frank, H. A.; Bocian, D. F. *Biochemistry* **1992**, 31, 11050–11058. Palaniappan, V.; Schenk, C. C.; Bocian, D. F. *J. Phys. Chem.* **1995**, 99, 17049–17058.
- (30) Czarniecki, K.; Diers, J. R.; Chynvat, V.; Erickson, J. P.; Frank, H. A.; Bocian, D. F. *J. Am. Chem. Soc.* **1997**, 119, 415–426.
- (31) Czarniecki, K.; Chynvat, V.; Erickson, J. P.; Frank, H. A.; Bocian, D. F. *J. Am. Chem. Soc.* **1997**, 119, 2594–2595.
- (32) Lyle, P. A.; Kolaczowski, S. V.; Small, G. J. *J. Phys. Chem.* **1993**, 97, 6924–6933. Small, G. L. *Chem. Phys.* **1995**, 197, 239–257.
- (33) Larsson, S.; Källebring, B. *Int. J. Quantum Chem., Quantum Biol. Symp.* **1990**, 17, 189–206.
- (34) Lathrop, E. J. P.; Friesner, R. A. *J. Phys. Chem.* **1994**, 98, 3056–3066.
- (35) Fleming, G. R.; Martin, J. L.; Breton, J. *Nature* **1988**, 333, 390–392.
- (36) O'Malley, P. J. *J. Am. Chem. Soc.* **1999**, 121, 3185–3192; *J. Phys. Chem. B* **2000**, 104, 2176–2182. O'Malley, P. J. *J. Am. Chem. Soc.* **2000**, 122, 7798–7801. O'Malley, P. J. *Chem. Phys. Lett.* **2000**, 331, 78–82.
- (37) Zhang, L. Y.; Friesner, R. A. *J. Phys. Chem.* **1995**, 99, 16479. Zhang, L. Y.; Friesner, R. A. *Proc. Natl. Acad. Sci. U.S.A.* **1998**, 95, 13603–13605.
- (38) Hutter, M. C.; Hughes, J. M.; Reimers, J. R.; Hush, N. S. *J. Phys. Chem. B* **1999**, 103, 4906–4915.
- (39) Blomberg, M. R. A.; Siegbahn, P. E. M.; Babcock, G. T. *J. Am. Chem. Soc.* **1998**, 120, 8812–8824. Siegbahn, P. E. M.; Blomberg, M. R. A.; Pavlov, M. *Chem. Phys. Lett.* **1998**, 292, 421. Zhang, X.; Ma, S.; Wang, Y.; Zhang, X.; Zhang, Q. *J. Photochem. Photobiol., A* **2000**, 131, 85–94.
- (40) Ceccarelli, M.; Lutz, M.; Marchi, M. *J. Am. Chem. Soc.* **2000**, 122, 3532–3533.
- (41) Reimers, J. R.; Hutter, M. C.; Hughes, J. M.; Hush, N. S. *Int. J. Quantum Chem.* **2000**, 80, 1224–1243.
- (42) Gunner, M. R.; Nicholls, A.; Honig, B. *J. Phys. Chem.* **1996**, 100, 4277–4291.
- (43) Klimkän, A.; Larsson, S. *Int. J. Quantum Chem.* **2000**, 77, 211–220.
- (44) Weiner, S. J.; Kollman, P. A.; Nguyen, D. T.; Case, D. A. *J. Comput. Chem.* **1986**, 7, 230.
- (45) Stewart, J. J. P. *J. Comput. Chem.* **1989**, 10, 209.
- (46) Dewar, M. J. S.; Zoebisch, E. G.; Healy, E. F.; Stewart, J. J. P. *J. Am. Chem. Soc.* **1985**, 107, 3902.
- (47) HyperChem (TM), Hypercube, Inc., 1115 NW 4th Street, Gainesville, Florida 32601.
- (48) Klevanik, A. V.; Shuvalov, V. A. *Dokl. Biophys.* **2000**, 373, 37–40.
- (49) Becke, A. D. *J. Chem. Phys.* **1993**, 98, 5648.
- (50) Frisch, M. J.; Trucks, G. W.; Schlegel, H. B.; Scuseria, G. E.; Robb, M. A.; Cheeseman, J. R.; Zakrzewski, V. G.; Montgomery, J. A., Jr.; Stratmann, R. E.; Burant, J. C.; Dapprich, S.; Millam, J. M.; Daniels, A. D.; Kudin, K. N.; Strain, M. C.; Farkas, O.; Tomasi, J.; Barone, V.; Cossi, M.; Cammi, R.; Mennucci, B.; Pomelli, C.; Adamo, C.; Clifford, S.; Ochterski, J.; Petersson, G. A.; Ayala, P. Y.; Cui, Q.; Morokuma, K.; Malick, D. K.; Rabuck, A. D.; Raghavachari, K.; Foresman, J. B.; Cioslowski, J.; Ortiz, J. V.; Stefanov, B. B.; Liu, G.; Liashenko, A.; Piskorz, P.; Komaromi, I.; Gomperts, R.; Martin, R. L.; Fox, D. J.; Keith, T.; Al-Laham, M. A.; Peng, C. Y.; Nanayakkara, A.; Gonzalez, C.; Challacombe, M.; Gill, P. M. W.; Johnson, B. G.; Chen, W.; Wong, M. W.; Andres, J. L.; Head-Gordon, M.; Replogle, E. S.; Pople, J. A. *Gaussian 98*, revision A.7; Gaussian, Inc.: Pittsburgh, PA, 1998.
- (51) Li, X.-Y.; Czernuszewicz, R. S.; Kincaid, J. R.; Spiro, T. G. *J. Am. Chem. Soc.* **1989**, 111, 7012–7023.
- (52) Thompson, M. A.; Zerner, M. C. *J. Am. Chem. Soc.* **1991**, 113, 8210. Thompson, M. A.; Zerner, M. C.; Fajer, J. *J. Phys. Chem.* **1991**, 95, 5693–5700. Thompson, M. A.; Schenter, G. K. *J. Chem. Phys.* **1995**, 99, 6374–6386.
- (53) Ridley, J.; Zerner, M. *Theor. Chim. Acta* **1973**, 32, 111; **1976**, 42, 323.
- (54) Myers, A. *Chem. Rev.* **1996**, 96, 911–926.
- (55) Spörlein, S.; Zinth, W.; Meyer, M.; Scheer, H.; Wachtveitl, J. *Chem. Phys. Lett.* **2000**, 322, 454–464.
- (56) Parson, W. W.; Chu, Z.-T.; Warshel, A. *Biochim. Biophys. Acta* **1990**, 1017, 251–272. Parson, W. W.; Nagarajan, V.; Gaul, D.; Schenk, C. C.; Chu, Z.-T.; Warshel, A. In *Reaction Centers of Photosynthetic Bacteria*; Michel-Beyerle, M. E., Ed.; Springer-Verlag: New York, 1990; pp 239–250. Alden, R. G.; Parson, W. W.; Chu, Z. T.; Warshel, A. *J. Am. Chem. Soc.* **1995**, 117, 12284–12298.
- (57) Brunschwig, B. S.; Logan, J.; Newton, M. D.; Sutin, N. *J. Am. Chem. Soc.* **1980**, 102, 5798. Christov, S. G. *Philos. Mag. B* **1985**, 52, 71–90.
- (58) Reimers, J. R.; Hush, N. S. *Chem. Phys.* **1989**, 134, 323–354.
- (59) Kestner, N. R.; Logan, J.; Jortner, J. *J. Phys. Chem.* **1974**, 78, 2148–2166. Ulstrup, J.; Jortner, J. *J. Chem. Phys.* **1975**, 63, 4358–4368. Jortner, J. *Biochim. Biophys. Acta* **1980**, 594, 193.
- (60) Klevanik, A. V. *Khim. Phys.* **2000**, 19, 27–35. Klevanik, A. V. *Khim. Phys.* **2000**, 19, 55–61.
- (61) Ritz, T.; Park, S.; Schulten, K. *J. Phys. Chem. B* **2001**, 105, 8259–8267.
- (62) Chan, C.-K.; Chen, L. X.-Q.; DiMagno, T. J.; Hanson, D. K.; Nance, S. L.; Schiffer, M.; Norris, J. R.; Fleming, G. R. *Chem. Phys. Lett.* **1991**, 176, 366–372.
- (63) Shochat, S.; Arlt, T.; Francke, C.; Gast, P.; van Noort, P. I.; Otte, S. C. M.; Schelvis, H. P. M.; Schmidt, S.; Vijgenboom, E.; Vrieze, J.; Zinth, W.; Hoff, A. J. *Photosynth. Res.* **1994**, 40, 55–66.
- (64) McAuley, K. E.; Fyfe, P. K.; Cogdell, R. J.; Isaacs, N. W.; Jones, M. R. *FEBS Lett.* **2000**, 467, 285–290. Fyfe, P. K.; McAuley-Hecht, K. E.; Ridge, J. P.; Prince, S. M.; Fritzsche, G.; Isaacs, N. W.; Cogdell, R. J.; Jones, M. R. *Photosynth. Res.* **1998**, 55, 133–140.
- (65) Finkle, U.; Lauterwasser, C.; Zinth, W.; Gray, K. A.; Oesterhelt, D. *Biochemistry* **1990**, 29, 8517–8521.
- (66) Nagarajan, V.; Parson, W. W.; Gaul, D.; Schenk, C. *Proc. Natl. Acad. Sci. U.S.A.* **1990**, 87, 7888–7892. Nagarajan, V.; Parson, W. W.; Davis, D.; Schenk, C. C. *Biochemistry* **1993**, 32, 12324–12336.
- (67) Apostolakis, J.; Muegge, I.; Ermler, U.; Fritzsche, G.; Knapp, E. W. *J. Am. Chem. Soc.* **1996**, 118, 3743–3752. Muegge, I.; Apostolakis, J.; Ermler, U.; Fritzsche, G.; Lubitz, W.; Knapp, E. W. *Biochemistry* **1996**, 35, 8359–8370.
- (68) Rischel, C.; Speidel, D.; Ridge, J. P.; Jones, M. R.; Breton, J.; Lambry, J. C.; Martin, J. L.; Vos, M. H. *Proc. Natl. Acad. Sci. U.S.A.* **1998**, 95, 12306–12311.
- (69) Van Brederode, M. E.; Jones, M. R.; van Mourik, F.; van Stokkum, I. H. M.; van Grondelle, R. *Biochemistry* **1997**, 36, 6855–6861. Van Brederode, M. E.; Ridge, J. P.; van Stokkum, I. H. M.; van Mourik, F.; Jones, M. R.; van Grondelle, R. *Photosynth. Res.* **1998**, 55, 141–146.
- (70) Van Brederode, M. E.; van Mourik, F.; van Stokkum, I. H. M.; Jones, M. R.; van Grondelle, R. *Proc. Natl. Acad. Sci. U.S.A.* **1999**, 96, 2054–2059.
- (71) Ando, K.; Sumi, H. *J. Phys. Chem. B* **1998**, 102, 10991–11000.